Preface

The field of imaging has been advancing steadily for the past several decades. During this time period, NASA was busy developing picture enhancement tools, while in Europe much attention was focused on morphological and surface analysis by means of image analysis. The introduction of the personal computers in the early eighties was also accompanied by the introduction of several powerful frame grabbers. The recent increases in computing power and scope as well as advances in software engineering resulted in the availability of desktop systems that are more capable than the large systems of the 70's and 80's. Imaging has already become a universal tool and continues to find applications in many areas of science and engineering. Image processing and image analysis have become common expressions and are recognized by a large fraction of the scientific community.

The field of imaging has provided the polymer scientists and the plastics industry with the necessary tools to evaluate parameters that were until recently difficult to quantify. In the fields of polymers, plastics, composites and textiles, such parameters include: texture, surface roughness, surface uniformity, fiber orientation distribution, fiber diameter distribution, rate of cracking, polymer blend morphology, dispersion of insoluble additives, corrosion, material weathering, and many other determinants of process and/or product quality. Most such observations were not possible until recently or at best pictorial standards were used for comparison purposes to assign arbitrary ranks to observed images. The advent of high-speed image acquisition coupled with dedicated software and digital signal processors is changing this state of affairs. The resulting data are often sufficient to characterize the physical properties of the materials, to quantify visual cues of images and to identify process related parameters controlling quality and production. These data allow process optimization to improve quality and/or throughput, to reduce the total number of substandard products, with concomitant cost savings.

This book contains a collection of papers that illustrate novel imaging techniques and image analysis methods currently in use to quantify the process or the material. The imaging techniques employed range from visible optical methods to scanning and transmission electron microscopy, x-ray, thermal wave infrared and atomic force microscopy. Image analysis is used to monitor/characterize a variety of processes. Examples of processes discussed include: extrusion, injection molding, foam production, film manufacture, compression molding, blow molding, vulcanization, melt spinning, reactive blending, welding, conveying, composite manufacture, compounding and thermosetting. Imaging techniques are also employed to characterize/quantify a number of important material properties. These include: fiber orienta-

tion distribution, homogeneity of mixing, the rate of spherulites growth, polymer crystallization rate, melt flow index, pore size and shape in foam, cell density in foam, void content, particle analysis in polymer blends, morphology, inter-particle distance, fiber diameter, fatigue crack, crazing, scratching, surface roughness, fiber length distribution, nucleation, oil penetration, peel adhesion, chemical resistance, droplet-fiber transition and others, electrical conductivity, dispersion and impurity content.

The broad collection of applications of imaging and image analysis techniques gathered in this book help illustrate material/process/property relationships for a wide selection of materials and processes. This book can serve as a valuable resource for the entire cross section of the plastics manufacturing industry.

Behnam Pourdeyhimi
North Carolina State University
Raleigh, May 1999

The Optimized Performance of Linear Vibration Welded Nylon 6 and Nylon 66 Butt Joints

V. Kagan, Siu-Ching Lui, G. R. Smith
AlliedSignal Inc.
J. Patry
Branson Ultrasonics Corp.

INTRODUCTION

The demand to use thermoplastics to replace metals in the automotive vehicle air induction systems has increased in recent years. For automotive under-hood applications such as air intake manifolds, air filter housings and resonators, the use of engineered plastics provides not only a savings in weight (up to 50 %) and in cost, but an increase in throughput. Joining of thermoplastics by vibration welding for such applications has been demonstrated for nylon 6 and 66.[1-3] It is estimated that 21.4 million air intake manifold components will be produced using such welding technology by the year 2010.[4]

The phenomenology and analysis of the welding process had been described previously.[5-9] There are four phases to vibration welding of thermoplastics: (1) heating of the interface by Coulomb friction; (2) unsteady melting and flow of material in the lateral direction; (3) melt zone establishment at a steady state condition; and (4) unsteady flow and solidification of the materials at the weld zone upon cessation of vibration.

It has been reported that for unreinforced materials, a weld strength nearly equivalent to the strength of base material can be attained.[10] However, for glass fiber reinforced thermoplastics, the maximum weld strength achievable is usually thought to be approximately equal to or less than that of the base material (i.e., the matrix) strength.[3] This lowered tensile strength is attributed to a change in the glass fiber orientation at the welded joint, so that fibers align along the weld line, perpendicular to applied stress in the tensile strength measurement. Figure 1 shows that the glass fiber does lie preferentially along the primary flow direction at the weld zone. The weld zone is typically very narrow and varies from 40 to 100 μm. Since

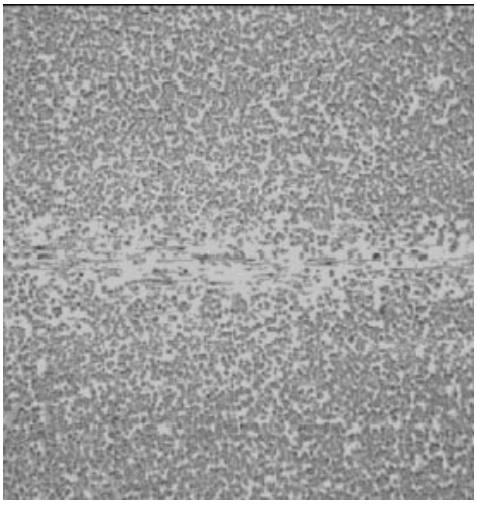

Figure 1. Orientation of glass fibers at the weld zone under non-optimized Welding conditions.

the glass fiber is no longer oriented in the tensile direction, a weld strength is achieved which is close to or less than that of the unreinforced polyamide (matrix).

For nylon 6 and 66, the maximum weld strength reported in the literature is 64.9 MPa.[1] In this paper, it was shown that when vibration welding parameters are optimized, a tensile strength of welded joint can be achieved up to 10-17% higher that of the non-reinforced material (matrix).

The goals of this study are to determine optimum conditions of glass fiber loading and to develop approaches which give significant strength increases at the weld zone beyond that of the matrix polymer.

WELDING PARAMETERS

Linear vibration welding of nylon 6 and 66 butt joints was performed at Branson Ultrasonics Corporation using a Mini-Vibration Welder. The welding parameters were as follows:

Maximum clamp load	4.5 kN
Weld Amplitude	1.02 to 1.80 mm
Weld time	4 - 25 seconds
Weld frequency	240 Hz

RESULTS AND DISCUSSION

Welding parameters such as pressure (loading), amplitude and time were varied to optimize tensile strength of the welded joints.[11,12] Only those samples which achieved a tensile strength higher than that of the base unfilled materials were selected to then study morphology of the weld zones. Details of the zone interface, fiber orientation, etc. were included in this analysis.[11] Optical microscopy was used to study the morphology of the samples, while image analysis was used to quantify fiber length.

ANALYSIS OF GLASS FIBERS LOADING AT WELD ZONE

The nominal fiber loading of the Capron nylon 6 injection molded part that were studied ranged from 0 to 50%. However, the actual fiber loading at the weld zone may vary if either fibers or the nylon matrix are preferably pushed away from the weld zone as the joint is

Table 1. Percentage of glass fiber in the flash for Capron 8233G HS (nylon 6)

Sample ID	Fiber in excess, wt%
1	32.04
2	32.52
3	32.26
4	32.56
5	32.54
6	32.20
7	31.93
average	32.29±0.25
8233 bulk	33.01±1.21

Table 2. Percentage of glass fiber loading in the flash for Capron 5233G HS (nylon 66)

Sample ID	Glas fiber in flash, wt%	Glass fiber in bulk, wt%
5233 EDG	33.48	33.94

formed. In order to determine whether the fiber loading in the excess flow region at the weld is different than in the bulk material, the weight % of fibers was measured by taking the weight difference of the excess before and after the matrix was pyrolized. The results of seven Capron 8233G HS nylon 6 samples processed under different welding conditions are summarized in Table 1. The results show that fiber loading of the various nylon 6 materials examined are approximately 0.5 to 1 wt% lower than the bulk composition.

For nylon 66, the glass content in the weld zone flash was measured from Capron 5233G HS nylon 66 samples. The results are given in Table 2 and show that fiber loading of nylon 66 at the weld zone flash are approximately 0.5 wt% lower than the bulk composition. These fiber content variations are rather small and are close to the accuracy of the fiber content measurement.

ANALYSIS OF GLASS FIBER LENGTH AT THE WELD ZONE

Table 3. Fiber length analysis on Capron 8233G HS

Sample ID	Number of fibers	Averaged length of fiber, μm
1	1775	124.7
2	1838	131.8
3	1106	151.9
4	1182	147.7
5	1018	167.8
6	1381	145.9
7	834	180.25
8233 bulk	1374	133.7

In order to determine whether there may be excessive breakage of fiber at the weld zone, an analysis of fiber length was conducted. Fiber length determination of fibers from the flash (recovered from pyrolysis ash) was measured by optical microscopy and by image analysis. Glass fiber samples were drawn from the ash and dispersed onto a glass slide with 2,2,2-trifluoroethanol (TFE) solvent. Ten optical micrographs were taken of each sample and a total of 1000-2000 fibers were digitized and measured by the image analyzer. Table 3 summarizes the results. The analysis indicates that averaged fiber

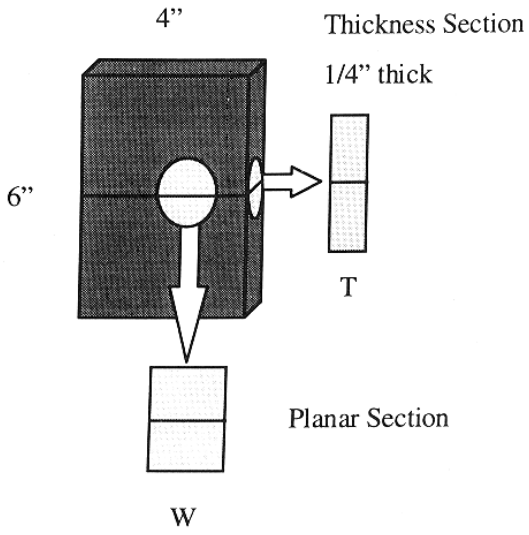

Figure 2. Sampling geometry.

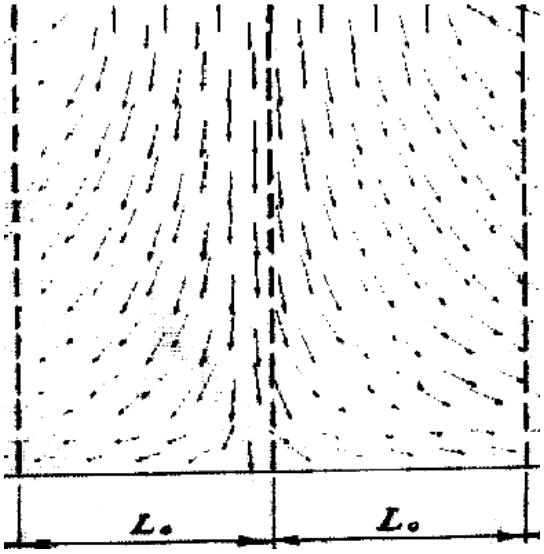

Figure 3. Schematic of glass fiber orientations in the molded plaque (the welding specimens were cut parallel to the width of the plaque).

lengths of all samples are within the range of 120 to 180 μm. This is comparable to the fiber length average of samples measured from the original molded tensile bars (away from the are of the weld zone).

Furthermore, a study of the weld zone fracture surface by scanning electron microscopy suggested that there is no excessive breakage of fibers at the weld zone.

ANALYSIS OF GLASS FIBER ORIENTATION DISTRIBUTION AT THE WELD ZONE

The fiber orientation distribution (FOD) of glass fibers at weld zone was studied by optical and scanning electron microscopy.[11] For each sample, both planar and through thickness sections were prepared and metallographically polished in preparation for optical microscopy study. Figure 2 depicts the sampling geometry for optical microscopy studies. Figures 3 and 4 are schematics of different glass fiber orientations (parallel, random or perpendicular) in the molded plaques prepared for welding. Micrographs at relatively low magnifications (25x and 50x) show the general FOD around the weld zone as well as fiber orientation at the weld zone. Figures 5-9 are optical micrographs taken from polished sections of nylon 6 samples with 6 wt% GF, 14 wt% GF, 25 wt% GF, 33 wt% GF and 50 wt% GF, respectively. Each micrograph

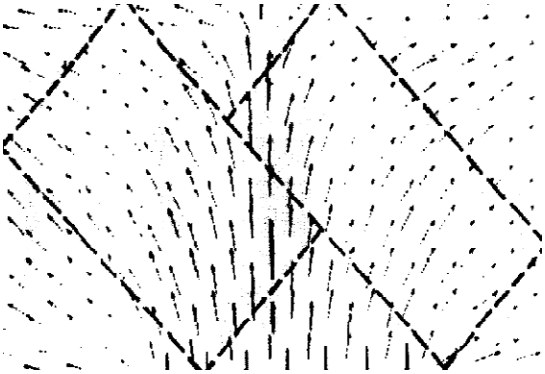

Figure 4. Schematic of glass fiber orientations in the molded plaque (the welding specimens were cut at 45 degree with respect to the length or width of the plaque).

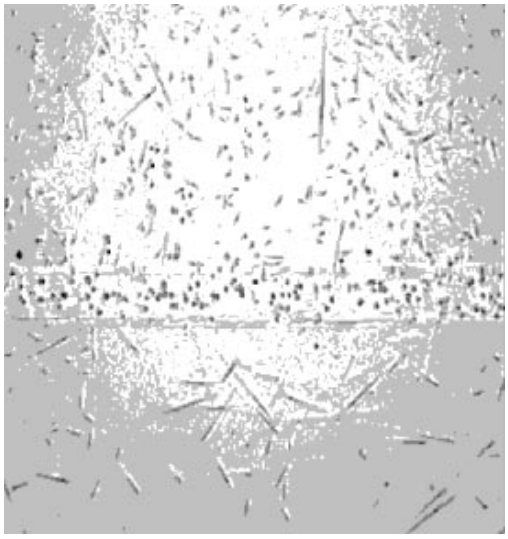

Figure 5. Optical micrograph of Capron® 8230G HS.

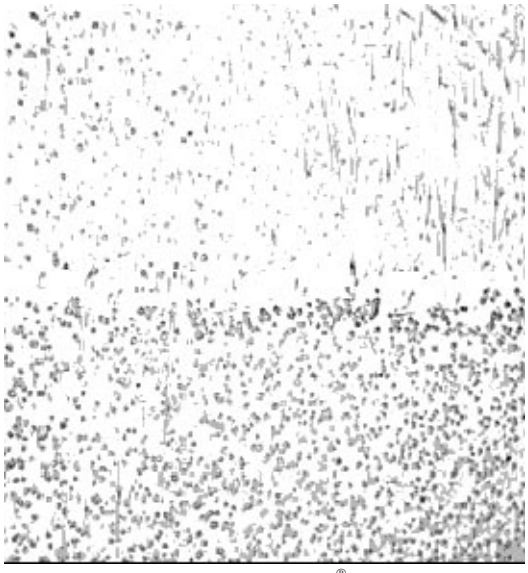

Figure 6. Optical micrograph of Capron® 8231G HS.

Figure 7. Optical micrograph of Capron® 8232G HS.

shows the fiber orientation both close to and away from the weld zone. Additionally the ap-

Figure 8. Optical micrograph of Capron 8233G HS.

Figure 9. Optical micrograph of Capron 8235G HS.

parent thickness of the weld zone can be measured directly from the FOD changes with position shown in the micrograph. Note that for samples with 14 and 25 wt% GF, there is apparent evidence of some fibers oriented in the tensile direction perpendicular to the weld plane.

It was noted that, in our tests, the effects of reinforcement at optimized welding conditions appeared independent of the glass fiber orientation in the molded plaques which were selected for welded - as suggested in Figures 6 and 7.

For the nylon 66 sample, only data from a 33 wt% glass filled material are presented here. Optical micrographs show a different weld zone morphology than was observed for nylon 6. The micrograph suggests that the weld zone is more difficult to define for the nylon 66 material, since the structural features at the weld zone are nearly the same as in the area adjacent to the weld zone. There is no notable fiber orientation in either the flow direction or the tensile direction, as was the case for nylon 6.

TENSILE STRENGTH OF WELD JOINTS

For each vibration weld condition (i.e., a set pressure, amplitude and weld time), ten specimens were tested under the standard ASTM D638M-93 tensile testing procedure for plastics.[13] Table 4 summarizes the results for weld line tensile strength. The influence of glass fiber loading on tensile strength is shown in Figure 10. These results indicate that all the weld joint samples in this study have a tensile strength higher than that of unreinforced nylon 6 (in-

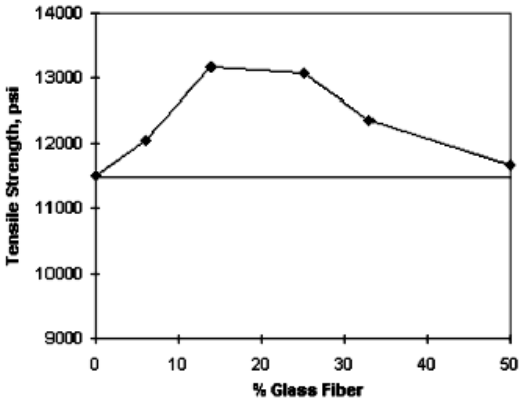

Figure 10. Tensile strength of weld joints (Nylon 6).

Table 4. Tensile strength of weld butt joints

GF, wt%	Trade name	Tensile strength, MPa
0	Capron™ 8202HS	79.3
6	Capron™ 8230G HS	83.1
14	Capron™ 8231G HS	90.7
25	Capron™ 8232G HS	90.2
33	Capron™ 8233G HS	85.2
50	Capron™ 8235G HS	80.5

dicated by the horizontal line). For the reinforced nylon 6 materials, the maximum tensile strength is 93.1 MPa. This occurs around 14 wt% to 25 wt% glass fiber loading. By comparison with the unreinforced material, which has a tensile strength of 79.3 MPa, this highest weld strength found in the reinforced grades represents a 17% increase in weld line tensile strength.

CONCLUSIONS

The tensile strength of welded nylon 6 materials appears to be slightly higher (approx. 4%) than that of welded nylon 66 under the same welding and reinforcing conditions. The study also shows that, at the interface, the glass fiber/nylon 66 composition is similar to that of the bulk composite.

The observed higher weld strength of the glass filled nylon 6 and nylon 66 (at certain compositions) and at optimum welding process conditions may be attributed to several factors:

1. For nylon 6, at some compositions and welding parameter choices, a percentage of the glass fibers appear to cross the weld plane at the interface, as suggested from optical micrographs.

2. The width of the weld zone, which is around 200-300 μm, is comparable to the average length of fibers. This may permit some mobility of the fiber to move in directions other

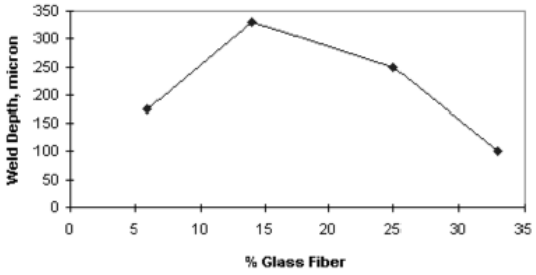

Figure 11. Variation of weld zone thickness.

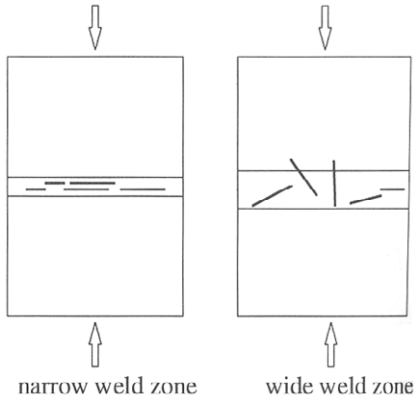

Figure 12. Schematic of fiber orientation in weld zone.

than the primary resin flow direction during the weld, i.e., the fibers are not so confined to move along the flow direction as in a narrow weld zone.

The weld zone thickness observed from the micrographs is plotted as a function of fiber loading in Figure 11. Note that the weld zone thickness does go through a maximum at 14 wt.% fiber loading. This maximum occurs at the same location (14 wt.% to 25 wt.%GF) as does the tensile curve maximum in Figure 10. This further suggests that the thickness of weld zone has a positive influence on the tensile strength of the welded joint. A schematic is shown in Figure 12 to represent what may be happening during welding of glass fiber reinforced polyamides.

3. By preparing weld specimens at different orientations to the predominant fiber orientation, studies of weld performance as a function of the glass fiber orientation distribution in the GF nylon 6 and 66 plaques were permitted. Results of this work suggest that, at the welding interface, the fiber orientation achieved in the region of the weld zone becomes independent of the predominant orientation of glass fiber in the bulk nylon 6, adjacent to the weld.

4. This study of linear vibration welded polyamide butt joints has shown an increase in tensile strength up to 35% in comparison with other published data.[1,3,10] The high tensile strength achieved in this study appear to be related both to some orientation of glass fiber at the interface (as observed for nylon 6) and to possible diffusion of nylon matrix at the interface (as in the case of nylon 66).

ACKNOWLEDGMENT

The authors wish to thank Caroline Bednarczyk for sample preparation and the microscopy study, Adam Haimes for his assistance in tensile testing, and Nanying Jia for preparing the computer graphics.

REFERENCES

1 Ian D. Froment, "Vibration Welding Nylon 6 and Nylon 66 - A Comparative Study", TWI, Cambridge, UK, ANTEC '95, p1285-1289 (1995).
2 S. M. Stevens, Technology Briefing, Dec 1993.
3 M. M. Matsco, "Multishell Technology for Plastic-Part Manufacture", Bayer Corp., Polymer Division, Proceedings of Structural Plastics '95, Technical Conference and New Product Design Competition, SPI, April 2-5, 1995.
4 Otto Altman, second Rosenheim Forum for Exhaust Systems and Throttle Plates, Plastic Forum. ASK Co., Rosenheim, Germany.
5 V. K. Stokes, "Vibration Welding of Thermoplastics, Part I: Phenomenology of the Welding Process", *Polymer Engineering and Science*, **28**, 718 (1988).
6 V. K. Stokes, "Vibration Welding of Thermoplastics, Part II: Analysis of the Welding Process", *Polymer Engineering and Science*, **28**, 728 (1988).
7 V. K. Stokes, "Vibration Welding of Thermoplastics, Part III: Strength of Polycarbonate Butt Welds", *Polymer Engineering and Science*, **28**, 989 (1988).
8 V. K. Stokes, "Vibration Welding of Thermoplastics, Part IV: Strengths of Poly(Butylene Terephthalate), Polyetherimide, and Modified Polyphenylene Oxide Butt Welds", *Polymer Engineering and Science*, **28**, 998 (1988).
9 C. B. Bucknall, I. C. Drinkwater, and G. R. Smith, "Hot Plate Welding of Plastics: Factors Affecting Weld Strength", *Polymer Engineering and Science*, **20**, 432 (1980).
10 H. Potente, M. Uebbing and E. Lewandowski, "The Vibration Welding of Polyamide 66", J. of Thermoplastic Composite Materials, 6, 2 (1993).
11 S. C. Lui, C. Bednarczyk and V. Kagan, "Vibration Welded Short Fiber Nylon Composites, Part I: Structure/Morphology" presented at the Polymer Technology Exchange Conference, Sept. 7th, 1995 at AlliedSignal, Morristown, NJ.
12 V.A. Kagan, S.-C. Lui, G.R. Smith, "The Effect of Fillers on the Vibration Welding of Nylon 6", p.48, ASM's Materials Congress, Cleveland, OH, 1995.
13 ASTM D638M-93, Standard Test Method for Tensile Properties of Plastics., 1995 Annual Book of ASTM Standards, Vol. 08.01, pp 65-73.

Image Analysis of Polypropylene Melt Fibre Stretching

M. T. Martyn and P. D. Coates
IRC in Polymer Science & Technology, Mechanical & Manufacturing Engineering, University of Bradford, Bradford UK

INTRODUCTION

Polymer melt spinning is an important melt conversion process used exclusively in the production of synthetic fiber. In the process melt deformation is predominantly through uniaxial extensional flow. The process and product quality are therefore governed by extensional characteristics of the melt. The extensional response of polymer melts is known to vary considerably. The diverse variation in extensional characteristics exhibited by melts is associated with differences in molecular topology. This leads to significant differences in the spinning performance between different polymer grades. An understanding of the effects of molecular topology on extensional rheology can play a key part in the development of new polymers and process optimization. This study is concerned with the measurement and interpretation of extensional flow behavior of polypropylene melts, with defined molecular characteristics, during a non-isothermal steady melt spinning operation.

The derivation of an apparent extensional viscosity from the melt spinning technique has been found useful in presenting and summarizing data.[1,2] The use of the technique to provide anything other than comparative data is largely discredited [3] largely because for a viscoelastic material the measurement does not provide a material property since at any instant in time the extensional histories of molecules along the drawn fiber are different and never actually achieve an equilibrium strain/strain rate. Consequently, 'extensional viscosity' derived from such a technique is often found to depend on experimental conditions.[4,5] It is for this reason that we have preferred to use total strain,[6] as a basis for comparing the extensional behavior of the melts.

ANALYSIS

In the spinning process, the melt is typically extruded vertically downwards, through a spinerette, and the resulting extrudate is simultaneously cooled by cross-flow air and stretched by the action of haul-off rollers. Conservation of mass requires a change in extrudate cross-sectional area when its velocity at the haul-off unit exceeds that through the orifice. The extrudate drawn down is controlled by haul-off velocity.

Extensional strain is derived from knowledge of the change in extrudate diameter with axial distance from the orifice exit. The axial tensile stress at any point along the drawn fiber can be calculated from a knowledge of the tensile force in the fiber and the fiber diameter at that point.

Analysis of the kinetics of the process is simplified for filaments of circular cross-section which decrease in diameter along the flow direction. Further simplifying assumptions are normally made, in particular that the melt is incompressible, deformation is purely by uniaxial tensile stresses (uniform velocity across the cross section), conditions are isothermal and flow is steady and axisymmetric.

From mass continuity, and assuming isothermal conditions, the velocity, V(x), of the extruded filament at some axial displacement, x, from the die exit is given by:

$$V(x) = 4\dot{m} / D(x)^2 \pi\rho \qquad [1]$$

from which the stretch rate, $\dot{\varepsilon}$, can be calculated as:

$$\dot{\varepsilon} = \frac{dV(x)}{dx} \qquad [2]$$

where $\dot{m}$ is the mass flow rate, D is the filament diameter and ρ is the melt density. For the purpose of this analysis the melt density was measured by PVT analysis using the Rosand RH7 rheometer, and determined to be approximately 770 kg/m^3 at 180°C for the melts investigated.

The tensile force, F_{ten}, acting on the filament can be calculated from the following force balance:[7]

$$F_{ten} = F_L + F_{gravity} - F_{drag} - F_{inertia} \qquad [3]$$

where, F_L is the measured tension on the filament, $F_{gravity}$ is the gravitational force which is calculated at a given axial displacement from the die exit and is given by the expression:

$$F_{gravity} = \int_{x}^{L} \rho g (\pi / 4) D(x)^2 dx \qquad [4]$$

The drag force, F_{drag}, acting on the filament while it is being stretched, can be calculated from the expression:[7]

$$F_{drag} = 0.843(\rho^{o} / \rho V(x)\dot{m})[\nu^{o}\pi\rho(L - x) / \dot{m}]^{0.915} \qquad [5]$$

where ρ^{o} and ν^{o} are the density and kinematic viscosity of the surrounding air respectively, and L is the distance from the exit of the die to the haul-off device. The inertial force, $F_{inertia}$, representing momentum imparted to the filament between the die exit and the haul-off device, is given by:

$$F_{inertia} = \dot{m}[V_{[L]} - V(x)] \qquad [6]$$

The line force, F_L, is the force as measured acting on the filament using a tensionmeter. Total Strain, ε, at any position, x, along the fiber is given by:

$$\varepsilon = \int_{0}^{t} \dot{\varepsilon}(s)ds = \int_{0}^{x} \frac{1}{V}\frac{\delta V}{\delta \zeta} d\zeta = Ln(V / V_0) \qquad [7]$$

The apparent extensional (spinning) viscosity is given by:

$$\lambda = \rho_c / \dot{\varepsilon} = [F_{ten} / A(x)] / dV(x)dx \qquad [8]$$

EXPERIMENTAL

The apparatus used in the investigation of the extensional behavior of melts consisted of a standard capillary rheometer with a controlled haul-off device as shown in Figure 1.

Details of the controlled rheology polypropylene melts investigated are given in Table 1. The molecular characteristics given were determined form GPC. Tests were performed at a melt temperature of 180°C using a constant rheometer crosshead velocity 6.66 mm/min., a haul-off speed of 6m /min and a capillary die with a diameter and length of 5.11 mm and 75 mm respectively.

The molten extrudate was subsequently drawn, non-isothermally, at a velocity ratio of 104 using the integral computer controlled haul-off device. The drawn fiber diameter profile

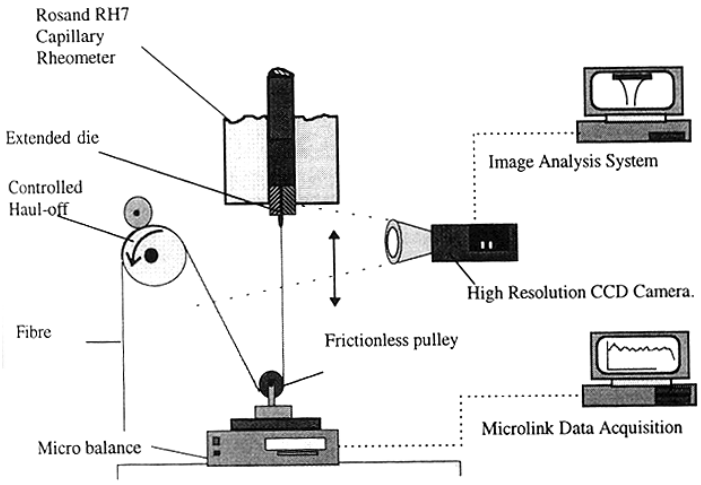

Figure 1. Schematic diagram of the melt fiber stretching apparatus.

Table 1. Molecular characteristics of the controlled rheology polypropylene melts studied

Polymers	MFI	M_w x 10^3	M_n x 10^3	M_w/M_n
A	3.0	433	34	12.7
B	5.5	299	30	10.1
C	10	233	30	7.6
D	21	180	27	6.8

was determined by measuring the fiber diameter at several displacements from the die exit using image analysis. In-house software was developed and used to digitize images of the drawn fiber and measure dimensions to an accuracy better than ±0.02 mm. Figure 2 shows a typical image of the drawn fiber. The imaging technique was compared and verified with measurements from a LaserMike™ micrometer in a limited number of tests.

The tensile force in the drawn fiber was calculated from the reactive force acting on a 4d microbalance supporting a frictionless guide pulley between the die and haul-off device. The output signal from the LaserMike and the micro balance attached to the pulley system on the apparatus were collected over a period of 300 s, using the Microlink 2000 data acquisition module and Windmill software. Data were averaged to produce values of fiber diameter and tensile force for each condition.

The true tensile force was determined after correcting for the effects of drag, inertia, and gravity on the fiber applying the analysis shown above. Diameter profiles were generated by curve fitting measured average diameters taken at several axial displacements. This was used to determine the total strain. Local spinning viscosity, λ, was then calculated from the tensile stress and stretch rate, ε, derived in turn from the diameter and draw ratio respectively.

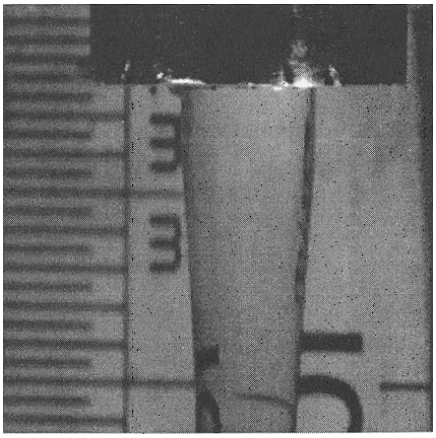

Figure 2. Typical image of the stretched fiber on exit from the die.

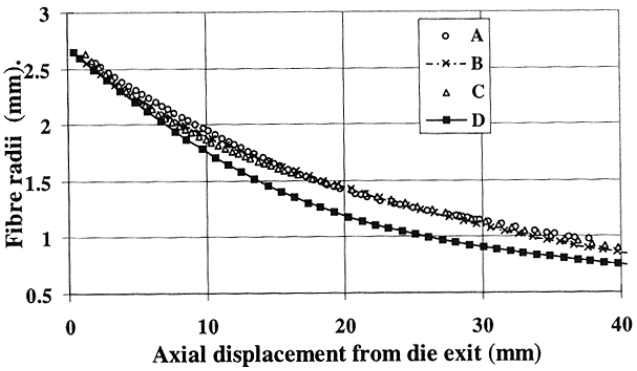

Figure 3. Draw down profile of various controlled rheology PP melts.

Table 2. Measured tensile force required to draw the PP melts at 6 m/min

Polymer	Tensile force, N
A	0.04338
B	0.04084
C	0.02925
D	0.02092

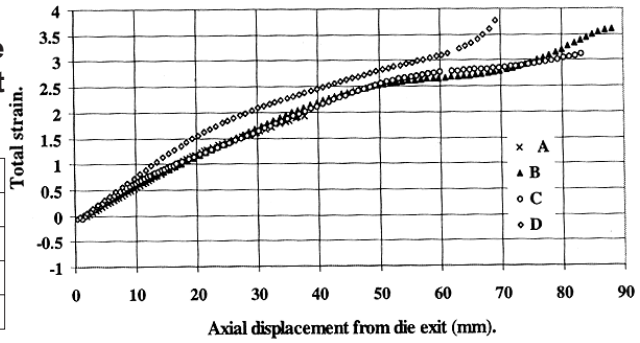

Figure 4. Variation of total strain with axial displacement for each melt.

RESULTS AND DISCUSSION

The diameter profiles derived from the digitized images of the stretched fiber are presented in Figure 3 along with a curve fitted profile of the same data. The draw down characteristics of the melts are influenced by the molecular weight, M_w, the lower the M_w the greater the initial (and subsequent) fiber draw down. This characteristic also produces a concomitant effect on the total strain profile of the fiber, as shown in Figure 4. All melts, with the exception of melt low M_w (melt D) behave in a similar manner with a near linear increase in total strain fol-

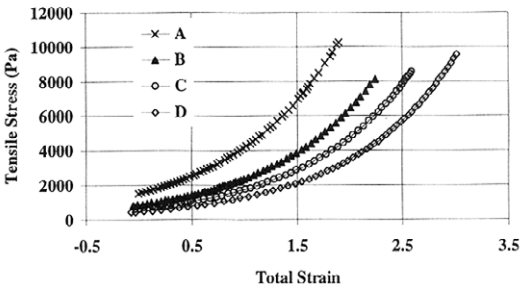

Figure 5. Stress - total strain relationship for the controlled rheology PP melts.

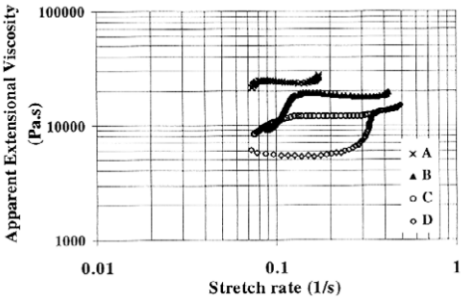

Figure 6. Variation of apparent extensional viscosity with total strain.

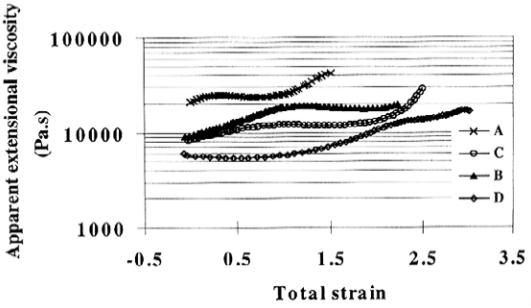

Figure 7. Variation of apparent extensional viscosity with stretch rate.

lowed by a plateau and further rapid rise in total strain. The latter rise in strain possibly reflects density changes with the onset of solidification.

The respective measured tensions required to draw down each melt at a constant haul-off rate are presented in Table 2. As would be expected the force required for draw down is dependent on the molecular characteristics, the higher the polymer M_w the greater the force. These values, together with a knowledge of the fibre diameter profile, were used to determine the tensile stress profile along each fibre. Tensile stress and strain relationships are presented in Figure 5. It can be seen that despite the lower draw down behavior of melts A and B the tension in the fibers of these melts is higher, at a given strain and particularly at large strains, than lower M_w melts.

Local apparent extensional (or spinning) viscosities are plotted against total strain in Figure 6. In general the data follow similar trends to those observed in strain-displacement profiles (Figure 4), namely exhibiting a plateau followed by rapid increase in viscosity. The high M_w melts A and B have similar extensional viscosities at small strains but the onset of strain hardening occurs at a lower total strain for the higher M_w melt A. The low M_w melt D has a significantly lower viscosity at low strain which gradually increases with strain.

As a comparison the apparent extensional (or spinning) viscosities of the melts are presented in the usual form, being plotted against strain rate, in Figure 7. The data has a similar trend to that of Figure 6 but with more pronounced strain hardening. Other studies[8,9] con-

ducted on commercial polypropylene homopolymers with wide molecular weight distributions, MWD, subjected to constant deformation rate conditions have shown that such polymers exhibit a decreasing 'extensional viscosity' with increasing strain rate. Han *et al.*,[1,10,11] have also studied commercial polypropylene homopolymers using the melt spinning method and found similar extensional thinning properties. However, Minoshima[12] studied narrow MWD polypropylene homopolymers under constant low deformation rates and noted that their extensional viscosities increased with extensional rate, in a similar manner to the melts studied in the above.

ACKNOWLEDGMENT

The support of EPSRC and the IRC in Polymer Science & Technology is gratefully acknowledged.

REFERENCES

1 C.D. Han, R.R. Lamonte, *Trans. Soc. Rheol.*, **16**, (3), 447, (1972).
2 N.E Hudson, J.E Ferguson, P. Mackie, *Trans. Soc. Rheol.*, **18**, 541 (1974).
3 K.M Baid, A.B. Metzner, *Trans. Soc. Rheol.,* **21**, 237, (1977).
4 M. Zidan, *Rheol. Acta*, **8**, 89 (1969).
5 C.A. Moore, J.R.A Pearson, *Rheol. Acta*, **14**, 436, (1975).
6 N.E Hudson, J.E Ferguson, *Trans. Soc. Rheol*., **20**, (2), 265 (1976).
7 A. Ziabicki; **Principles of Melt Spinning**, Vol 1. Ed. H.F. Mark, *Wiley*, New York , (1957).
8 J.L. White, *J.Soc. Rheol. Jpn.*, **4**, 137, (1976).
9 J.L. White, Y. Ide, *J. Appl. Polym. Sci*., **22**, 1061, (1978).
10 C.D. Han, R.R. Lamont, *J. Appl. Polym. Sci*., **16**, 3285, (1972).
11 C.D. Han, K.W. Kim, *J. Appl. Polym. Sci.*, **20**, 1555, (1976).
12 W. Minoshima, M.Sc. Thesis Poly. Engn. University Tennesse, 1978.

The Effect of Fiber Orientation and Distribution on the Tooth Stiffness of a Polymer Composite Gear

D. J. Weale, J. White and D. Walton
School of Manufacturing and Mechanical Engineering, The University of Birmingham, Edgbaston, Birmingham B15 2TT, UK

INTRODUCTION

The advantages and disadvantages of plastic gears are fairly well established. The main advantages are their low cost of manufacture when produced by injection molding, low noise and high resilience, good bearing capacity and the ability to run unlubricated. The main disadvantage is that they have much lower power ratings and life compared with lubricated metal gears. The use of fiber reinforcement and internal solid lubrication has significantly enhanced their load carrying capacity and their wear performance. Fundamental research on short fiber reinforced composites has concentrated on tribological aspects.[1] This work is almost exclusively based on simple roll/slide and pin-on-disk testing which, while being useful, has limited relevance for plastic gears.

The effect of fibers beneath the surface and in the bulk of the tooth on stiffness has not previously been studied. Indeed, obtaining data on the elastic constants for use in Hertzian contact and deflection calculations has proven difficult if not impossible in the past. This paper examines the FOD and offers a method of establishing elastic properties and quantifying the accuracy of these values for a plastic gear.

FIBRE ORIENTATION AND DISTRIBUTION OF A POLYMER COMPOSITE GEAR

The fibre orientation and distribution within an injection molded component is a function of many parameters, these include:

- Component geometry,
- Molding conditions such as gating, temperature, pressure and holding time,

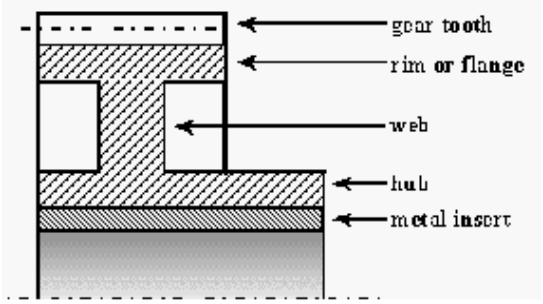

Figure 1. Section through a test gear.

- Matrix material,
- Polymer melt viscosity,
- Fibre type, including aspect ratio, density and volume fraction.

In a typical plastic gear geometry a number of complicated geometrical features are present. It is quite common for plastic gears to be designed with webs and rims because of the need to keep sections of uniform size and hence to minimize post mold distortion. These features must have a dominating effect on the resulting FOD. The shear forces within a melt, at such features, tend to produce some form of fibre alignment, Figure 3(b), whereas fibers away from these surfaces tend to orientate themselves in a more random fashion. Figure 1 shows a diagram of a cross section through the test gear used in this study. It is a typical plastic gear form which incorporates a hub, web and rim.[2] The gears in this study were injection molded using diaphragm gating. The melt was injected via the hub, through the web into the rim and finally filled the teeth. A qualitative examination, using scanning electron microscopy, has been made of a such a gear molded from nylon reinforced with short glass fibers. This analysis indicated that the FOD on the gear flank is approximates to a 2D random pattern, shown in Figure 2, and that a 3D random pattern is established within the gear body. There is also some alignment along the facewidth caused by the melt flow which enters the teeth through the web in the middle, and flows in the axial direction filling the tooth. Closer inspection shows that fibers can lie on the exposed surface of the gear flank, and may therefore cause tribological problems.

DETERMINATION OF ELASTIC PROPERTIES

The overall FOD is, in reality, a complex 3D pattern and these observations simply represent general trends within the gear tooth. The variation in FOD obviously results in a variation in the mechanical properties. Relating these qualitative findings to the resulting mechanical properties is a complex issue.

MANUFACTURERS' DATA

Published data on the mechanical properties of injection molded composites are available, e.g. LNP, a materials supplier, lists elastic moduli for a range of composite materials.[3] However, their data is based on tests involving simple test specimens which will have little in com-